NOTES AND CORRESPONDENCE

Gradient Balance in Tropical Cyclones

H. E. WILLOUGHBY

Hurricane Research Division, AOML/NOAA, Miami, Florida

31 January 1989 and 5 September 1989

ABSTRACT

Analysis of a large inventory of in situ observations from research aircraft shows that the gradient wind approximates the axisymmetric swirling flow in the free atmosphere within 150 km of the centers of Atlantic hurricanes and tropical storms. In the middle and lower troposphere, the rms difference between the azimuthal mean swirling and gradient winds is typically <1.5 m s^{-1} with zero bias. This balance prevails only for the azimuthal mean, not locally, nor is balance to be expected in either the surface friction layer or the upper tropospheric outflow layer where the radial flow is comparable with the swirling flow.

It is theoretically possible that axisymmetric supergradient flow may occur in response to rapid radial acceleration where the radial flow slows in the friction layer beneath the eyewall or where it converges into intense diabatically forced updrafts. Nevertheless, the observations in the free lower and midtroposphere show that systematic departures of the azimuthal mean vortex from balance are too small to measure.

1. Introduction

A companion paper (Willoughby 1990) confirms earlier observations (Willoughby et al. 1982) of convective rings—contracting annuli of strong swirling wind and cumulonimbus that play a key role in hurricane intensification. The eyewall is an example of a convective ring. A simple model of balanced vortex response to added heat or momentum (Eliassen 1952) appears to explain convective ring contraction (Smith 1981; Shapiro and Willoughby 1982; Schubert and Hack 1982), but if one wants to apply this model to hurricanes, the axisymmetric flow must be balanced.

Observational studies arguing for gradient or thermal wind balance in tropical cyclones (LaSeur and Hawkins 1963; Hawkins and Rubsam 1968; Willoughby 1979; Jorgensen 1984) contradict those arguing against it (Gray 1962, 1967; Gray and Shea 1974). The issue of balance is important theoretically not only because the balanced model explains the dynamics of convective rings, but also because it provides tidy explanations for other observed features of the axisymmetric vortex: outward slope of the eyewall, descent inside the eye, and deep lower-tropospheric inflow outside the eye (Palmen 1956; Eliassen 1959; Willoughby 1988b). In the nearly balanced model, horizontal gradients of latent heat release force the axisymmetric secondary (radial and vertical) circulation in the hurricane core above the boundary layer, particularly the thermally indirect descent within the eye. This explanation contrasts with the view that the descent arises because diffusion of angular momentum into the eye causes supergradient winds that centrifuge air out of the eye at low levels (Malkus 1958; Kuo 1959). The supposed observations of supergradient winds in the eyewall have been, at least implicitly, a factor in uncritical acceptance of the latter explanation (e.g., Carrier et al. 1971; Emanuel 1988).

The observational studies disputing balance have apparent defects. The Doppler aircraft navigation used before the mid-1970s provided less accurate winds and positions than does modern inertial navigation equipment (INE). The composite analysis of Gray and Shea (1974) positioned the data relative to the radius of maximum wind rather than with respect to absolute radius. This procedure exaggerated any nonbalanced asymmetries. Gray (1962) analyzed balance locally rather than in the axisymmetric mean and neglected the local acceleration in fixed coordinates caused by the hurricane's motion. These errors, combined with a confused treatment of the transformation into moving coordinates, made it appear that large imbalances—explained in terms of eddy cumulus fluxes (Gray 1967)—prevailed in tropical cyclones.

This paper resolves the controversy in favor of widespread balance by comparison between observed axisymmetric swirling winds and gradient winds, although it recognizes that agradient winds may arise through strong frictionally or diabatically induced radial accelerations.

2. Observations of gradient balance

This section compares azimuthally averaged tangential winds with gradient winds in some of the trop-

Corresponding author address: Dr. Hugh E. Willoughby, NOAA/AOML/HRD, 4301 Rickenbacker Causeway, Miami, FL 33149.

ical storms and hurricanes described by Willoughby (1990). The analysis depends upon statistical estimation of radial profiles the time-mean, axisymmetric swirling wind and isobaric height ($\bar{V}$ and $\bar{Z}$, "the intercepts") and rates of temporal change of the same quantities (α_V and α_Z, "the slopes"). The intercepts and slopes approximate the evolution of the axisymmetric vortex as a linear change with time and are functions of radius. They are expressed in terms of spline curves fitted to observations obtained at flight level as the aircraft flew repeatedly into or out of the cyclone center. Details of the analysis appear in Willoughby (1990).

Typically, the analysis treats observations from a single aircraft sortie—one flight by one aircraft making 8 to 20 penetrations or exits of the eye at fixed altitude during 5 to 7 h—as a unit. In slowly developing cyclones, however, two or three sorties are sometimes combined. To facilitate comparisons, the slopes are expressed as the change expected over a 6 h interval. Thus, if observations were taken during two sorties flown over 13 h, the slope would represent $^6/_{13}$ of the total change. In the figure captions and Table 1, each sortie is denoted by an identifier, for example 840831H. The first pair digits indicate the year; the second pair is the month; the last pair is the day (UTC) on which the flight began; and the letter denotes the individual WP-3D aircraft: H for N42RF and I for N43RF. Thus, 840831H represents a flight on the last day of August 1984 by N42RF.

Wind and isobaric height are the variables of interest. The observed wind is the vector difference between the motion of the aircraft through the air, measured by pitot tubes and airframe attitude sensors, and that with respect to the earth, measured by the INE. The isobaric height is calculated from pressure at flight level, measured by an aneroid sensor, and geometric altitude, measured by the radar altimeter. Apart from common navigation and common pressure between the aneroid and the static side of the pitot tube, wind and isobaric-height measurements are independent.

The time-mean cyclostrophic wind, $\bar{V}_c$, derives from radial differentiation of the spline curve for the isobaric-height intercept:

$$\bar{V}_c = \left[gr \frac{\partial \bar{Z}}{\partial r} \right]^{1/2}. \tag{1}$$

$\bar{V}_c$, in turn, relates to the gradient-wind intercept, $\bar{V}_g$, by:

$$\bar{V}_g = \bar{V}_c R_c \left[\frac{1}{2} + \left(\frac{1}{4} + R_c^2 \right)^{1/2} \right]^{-1}. \tag{2}$$

The gradient wind slope is

$$\left[\frac{2\bar{V}_g}{r} + f \right] \alpha_g = g \frac{\partial \alpha_Z}{\partial r}. \tag{3}$$

Here g is the acceleration of gravity; r is distance to the vortex center; f is the Coriolis parameter; and R_c is the local cyclostrophic Rossby number, $\bar{V}_c/fr$. Since R_c is generally ≥ 10 near the radius of maximum wind (RMW), $\bar{V}_c$ approximates $\bar{V}_g$ closely. The following discussion compares $\bar{V}$ with $\bar{V}_g$ and α_V with α_g in tropical cyclones that range from tropical storms to extreme hurricanes.

Figure 1 illustrates gradient balance in tropical storms Arthur of 1984 and Elena of 1985. Arthur dissipated without reaching hurricane strength, but Elena developed—albeit slowly—into a major hurricane. In both storms, the radial pressure gradient was fairly uniform, supporting a flat wind profile. Quantitative measures of the differences between the gradient and actual winds appear in Table 1. The root-mean-square (rms) difference between $\bar{V}_g$ and $\bar{V}$ was about 20% of the $\bar{V}$ in Arthur and 10% of $\bar{V}$ in Elena; an average bias made $\bar{V}$ stronger in both storms.

Here and subsequently, $\bar{V}_g$ fluctuated much more than $\bar{V}$ because the spline curves exhibited a ripple due to uneven data coverage. When, for example, one radial pass was shorter than the others, the fitting algorithm responded to the discontinuity in the data by generation of a ripple at wavelengths just longer than

TABLE 1. Summary of maximum swirling wind and differences between the swirling and gradient winds in m s^{-1}. The bias and rms values for the entire sample are averages of the individual entries weighted by the number of profiles. V_{max} for the sample is a simple average.

					Wind		Change	
Cyclone	Flight	Sorties	Profiles	V_{max}	Bias	Rms	Bias	Rms
Alicia	830817I	1	12	31	−0.08	1.30	−0.21	4.80
Alicia	830817H	1	14	39	0.35	1.13	2.39	3.46
Arthur	840831H-840902H	3	22	8	0.69	1.72	−0.41	1.12
Danny	850814I-850815H	2	20	23	0.01	1.54	−0.13	1.55
Diana2	840911I	1	14	42	0.00	0.85	0.44	1.46
Diana2	840911H	1	16	52	−1.22	1.75	0.40	1.71
Diana2	840912H	1	14	44	−0.47	0.86	0.85	2.05
Elena1	850829I	1	12	24	0.83	1.46	−0.94	6.36
Elena2	850901I	1	14	48	−0.29	1.18	−1.56	2.53
Gloria3	850926H	1	14	38	0.13	1.06	0.87	2.44
Sample		13	152	35	−0.01	1.36	0.17	2.94

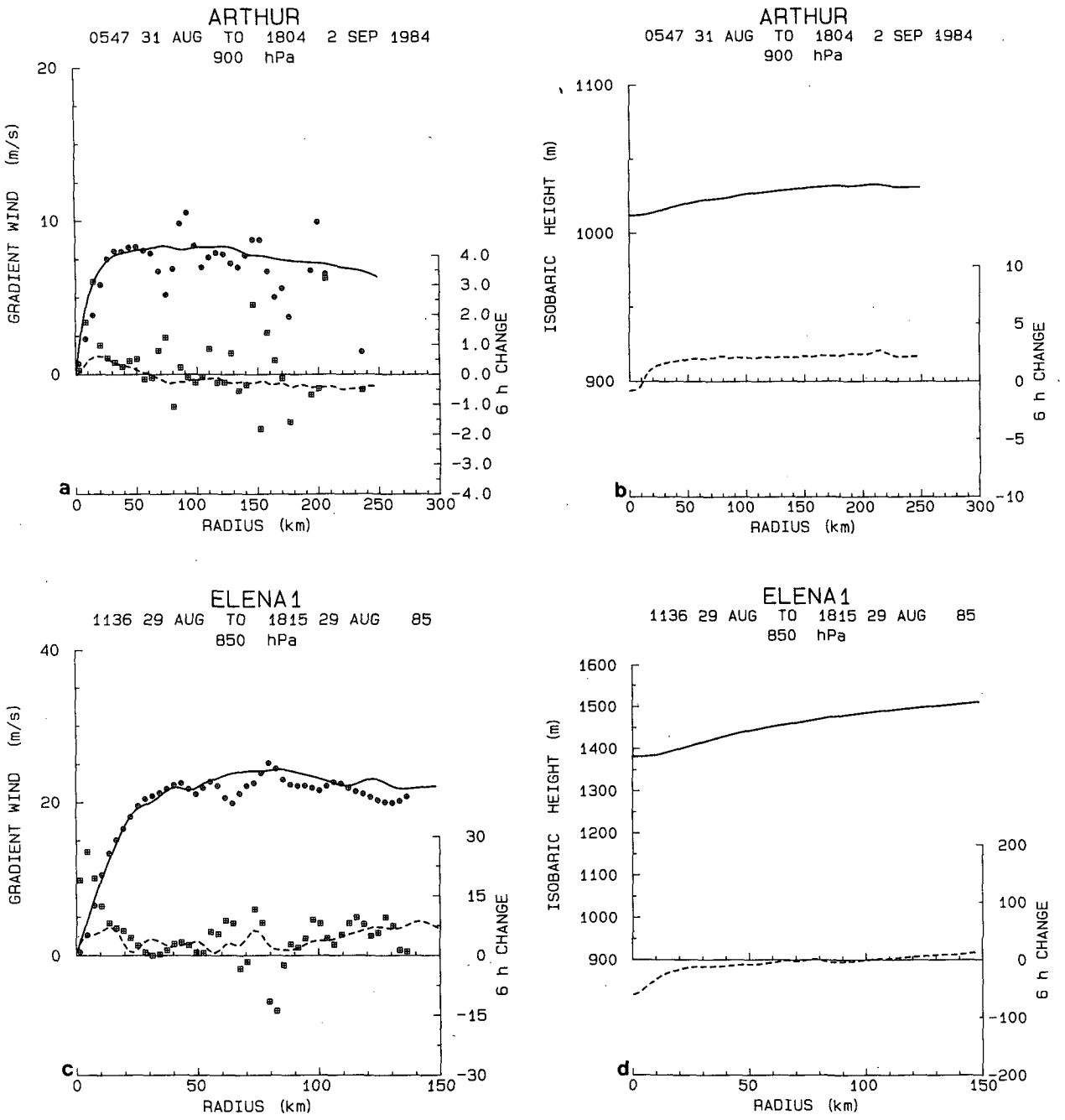

FIG. 1. (a) Gradient balance in tropical storm Arthur observed during flights 840831H, 840901H, and 840902H. The solid curves are the time mean axisymmetric swirling wind; the dashed curves are the swirling wind's change in 6 h; the circular plotted points are the gradient wind; and the square points are the gradient wind's rate of change. (b) The isobaric height corresponding to (a); the solid curve is the height of the isobaric surface nearest flight level, and the dashed curve is the 6 h height change. (c) and (d) Gradient balance and isobaric height observed during flight 850829I in Elena when it was a tropical storm. The plotted points in (a) and (c) are related to the curves in (b) and (d) through (1) and (2).

the cutoff of the inherent smoothing. Although the ripple was nearly imperceptible in $\bar{Z}$ and α_Z, differentiation to obtain the radial pressure gradient accentuated it in $\bar{V}_g$ and α_g. The ripple was prominent in samples containing few (<8) radial profiles of differing length, but less so in those containing many profiles (>16) of nearly the same length.

The temporal changes of the observed and gradient winds did not agree so well as the mean values because the change of the gradient wind depended upon the

time derivative of the radial derivative of isobaric height. Although the rms difference between α_g and α_V was comparable with α_V itself, α_g and α_V had some qualitative features in common. In both storms, the height fell near the center, supporting increases of the swirling wind around the center. The absolute values of α_V were larger in Elena than in Arthur. In Elena, the radial gradient of α_Z supported wind increases throughout the domain; whereas outside the immediate center of Arthur, the radial gradient α_Z reversed so that the outer vortex weakened with time.

Figure 2 shows Hurricanes Alicia of 1983 and Danny of 1985 as they reached the threshold of hurricane strength. The winds and isobaric height gradients were stronger than in the tropical storms. The rms difference between $\bar{V}_g$ and $\bar{V}$ was slightly smaller in absolute magnitude than in the tropical storms, but it represented only 3%–5% of the stronger hurricane winds. In Alicia

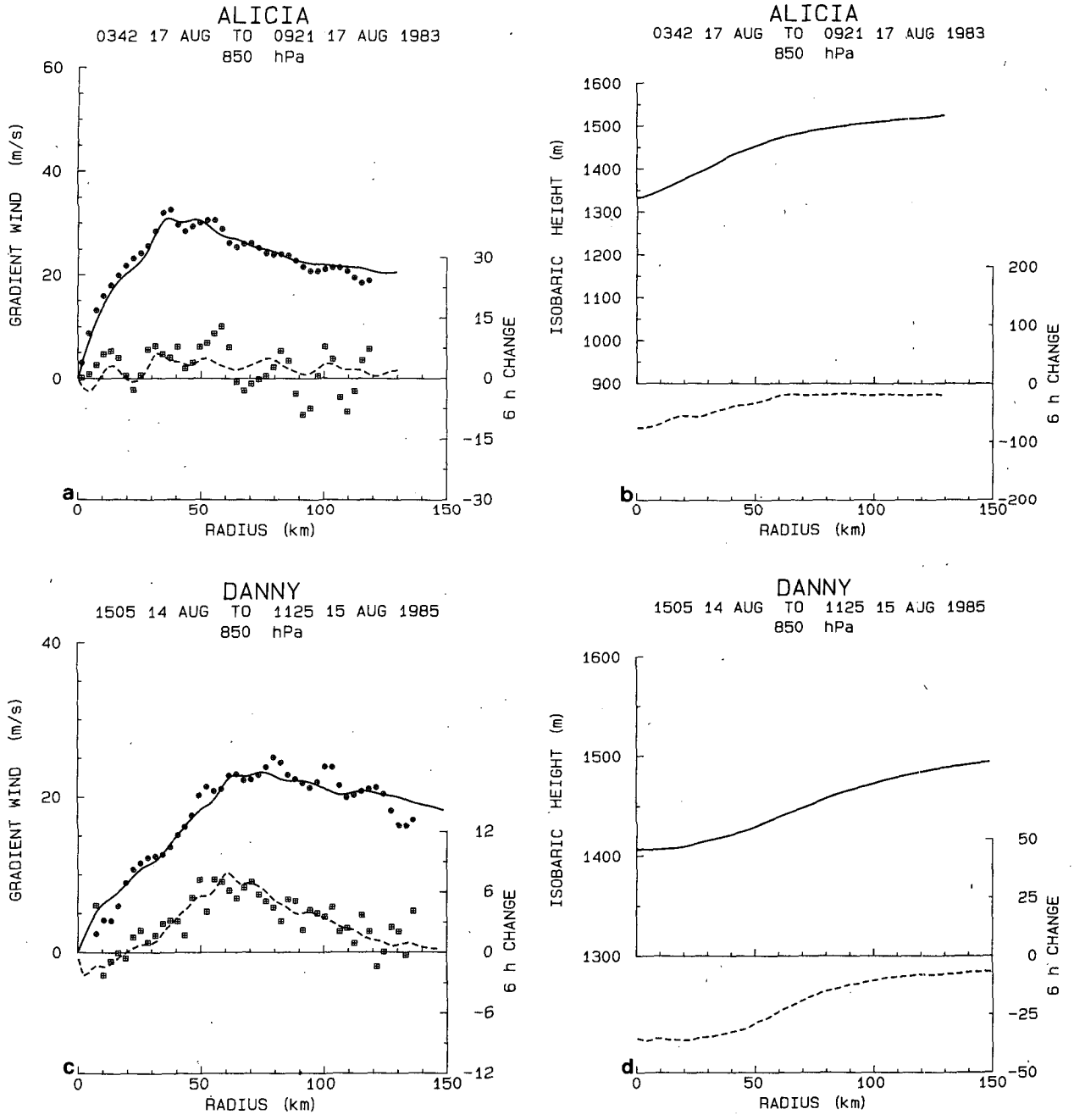

FIG. 2. Tropical storms reaching hurricane intensity: (a) and (b) gradient balance and isobaric height observed during flight 830817I in Alicia; and (c) and (d) during flights 850814I and 850815H in Danny. Data are represented in the same way as in Fig. 1.

at this stage, the rms difference between α_g and α_V remained comparable with α_V; but in Danny, the rms error was only 20% of the maximum α_V. In Alicia gradient of height falls was broad so that the wind increases extended outside the eye; but in Danny the isobaric height falls were concentrated inside the RMW and had a strong radial gradient across the eyewall. The wind increased most rapidly inside the RMW, but it also increased at the RMW, causing the maximum swirling wind, $\bar{V}_{max}$, to increase as the RMW contracted.

Figure 3 shows Diana of 1984 and Elena as they became intense hurricanes. The rms difference between $\bar{V}_g$ and $\bar{V}$ was 2% of $\bar{V}_{max}$, and that between α_g and α_V was 10% of the maximum α_V in Diana and 20% in Elena. The larger difference in Elena arose because α_g was nearly zero outside the RMW; whereas α_V was slightly negative, causing a bias difference > 1 m s^{-1}.

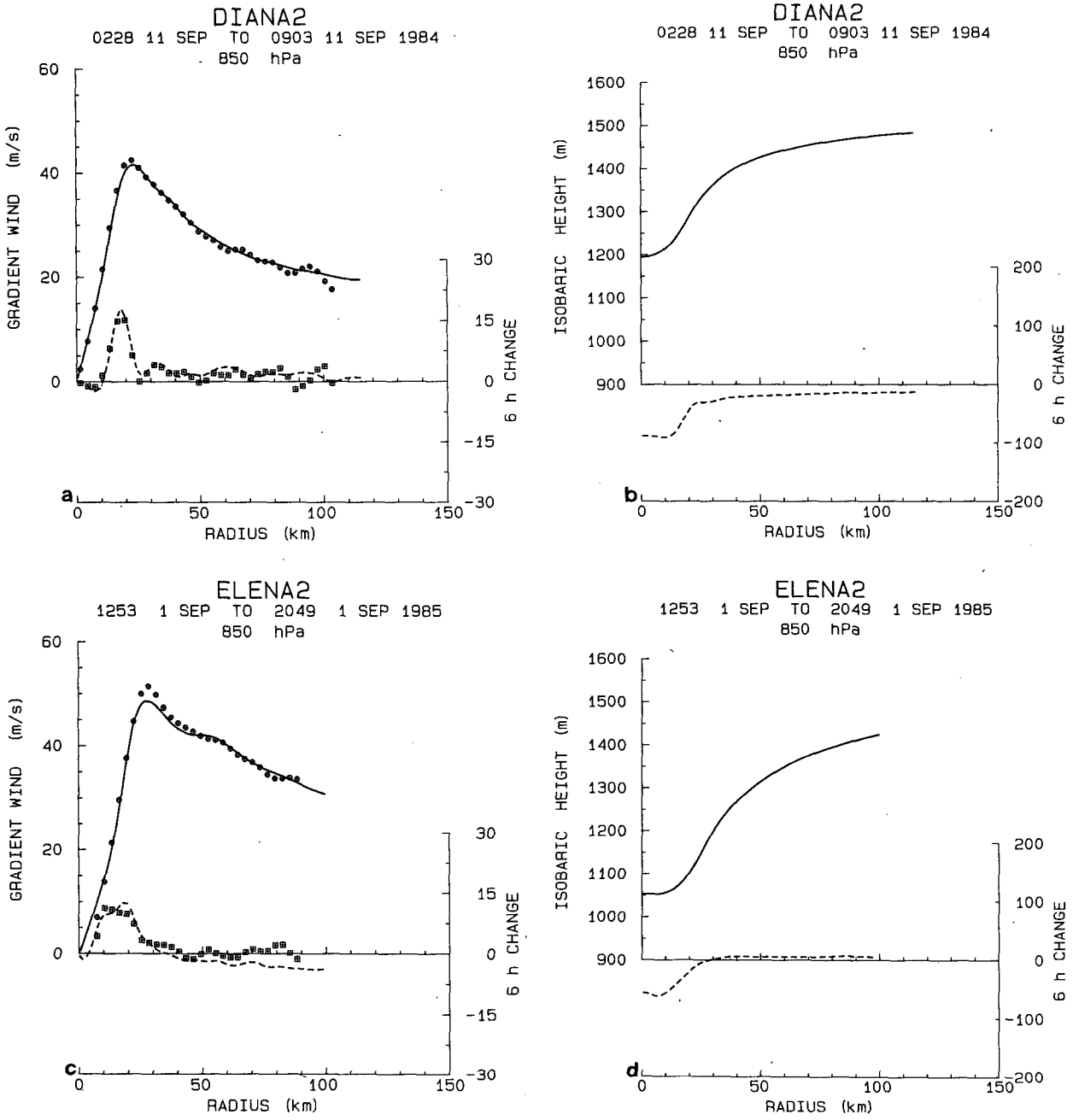

FIG. 3. Rapidly intensifying hurricanes: (a) and (b) gradient balance and isobaric height observed during flight 840911I in Diana; and (c) and (d) during flight 850901I in Elena. Data are represented in the same way as in Fig. 1.

The greater intensity in Fig. 3 produced the following differences from Fig. 2: the wind maxima were sharper, the height falls were more concentrated inside the RMW, and the rapid wind strengthening on the inward side of the wind maximum was more pronounced. In qualitative terms, these observations agree closely with the predictions of the balanced-vortex model and bear a striking resemblance to Hurricane Allen on 8 August 1980 (Willoughby et al. 1982).

In intensifying tropical cyclones, outer convective rings are often observed to form around the preexistent eyewalls. Figure 4 illustrates this phenomenon in Alicia and Diana. In both hurricanes, the inner convective ring continued to strengthen as the outer one formed. The gradients of isobaric height fall were concentrated at and inside the convective rings, sustaining two annuli of increasing winds. Between the rings, the isobaric height gradient decreased with time, causing the winds

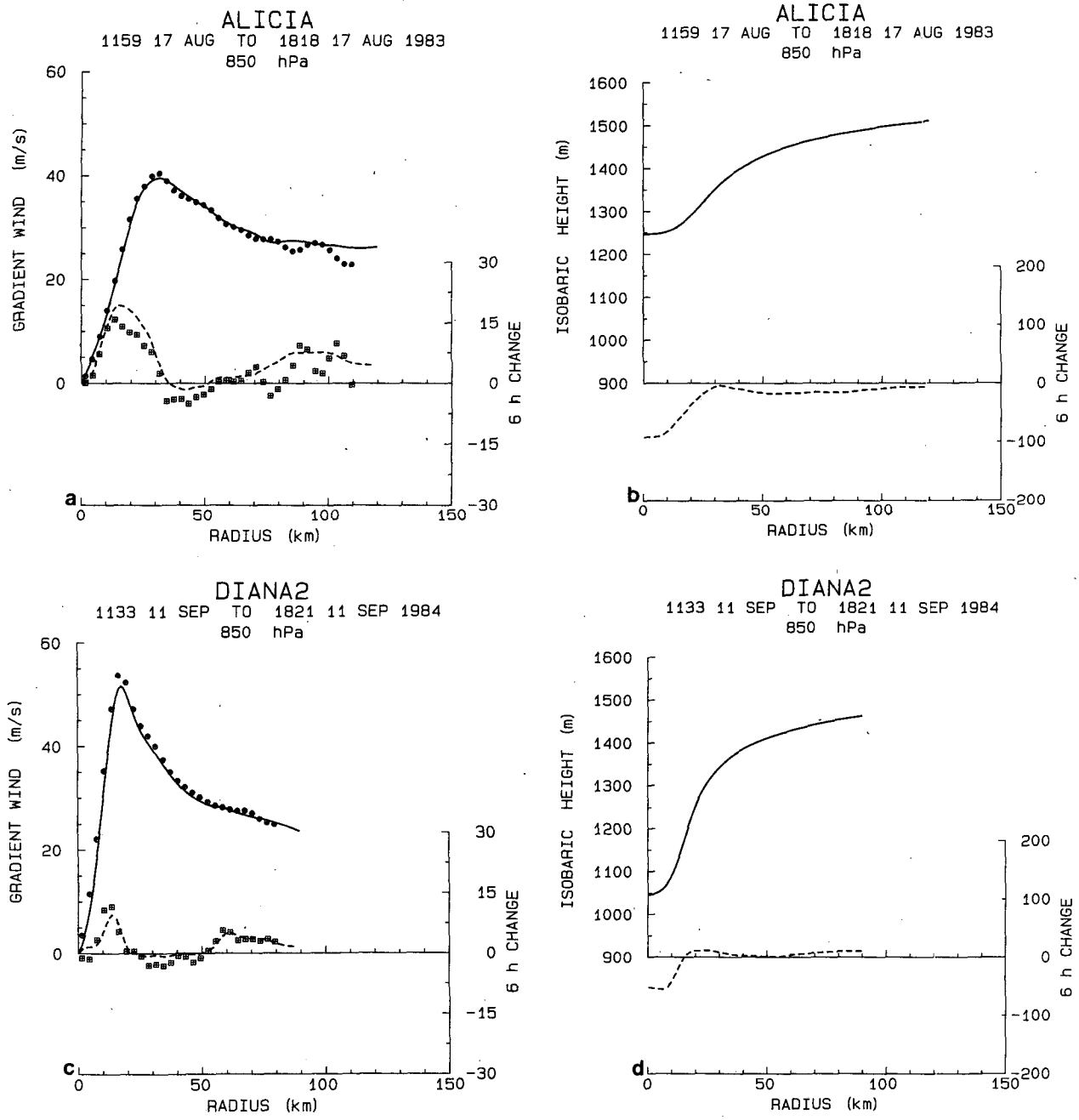

FIG. 4. Hurricanes with concentric eyewalls: (a) and (b) gradient balance and isobaric height observed during flight 830817H in Alicia; and (c) and (d) during flight 840911H in Diana. Data are represented in the same way as in Fig. 1.

to decrease. The winds remained in gradient balance throughout the process. The rms differences between $\bar{V}_g$ and $\bar{V}$ were 3% of $\bar{V}_{max}$ in both hurricanes, and those between α_g and α_V were 14% and 24% of the maximum α_V in Alicia and Diana, respectively.

Alicia made landfall just as the inner eyewall began to weaken but, as Fig. 5a shows, the wind at Diana's outer ring strengthened while rising isobaric heights near the vortex center caused decreasing winds at the original RMW. In Hurricane Gloria of 1985, the outcomes of a concentric eyewall replacement were a broad radial gradient of isobaric height and a flat wind profile (Fig. 5c). Gloria's primary circulation resembled the tropical storms in Fig. 1, but with twice as much wind. The isobaric heights fell slowly throughout the domain. Convection immediately around the center and in a partial convective ring beyond 100 km radius sharpened local isobaric height gradients and

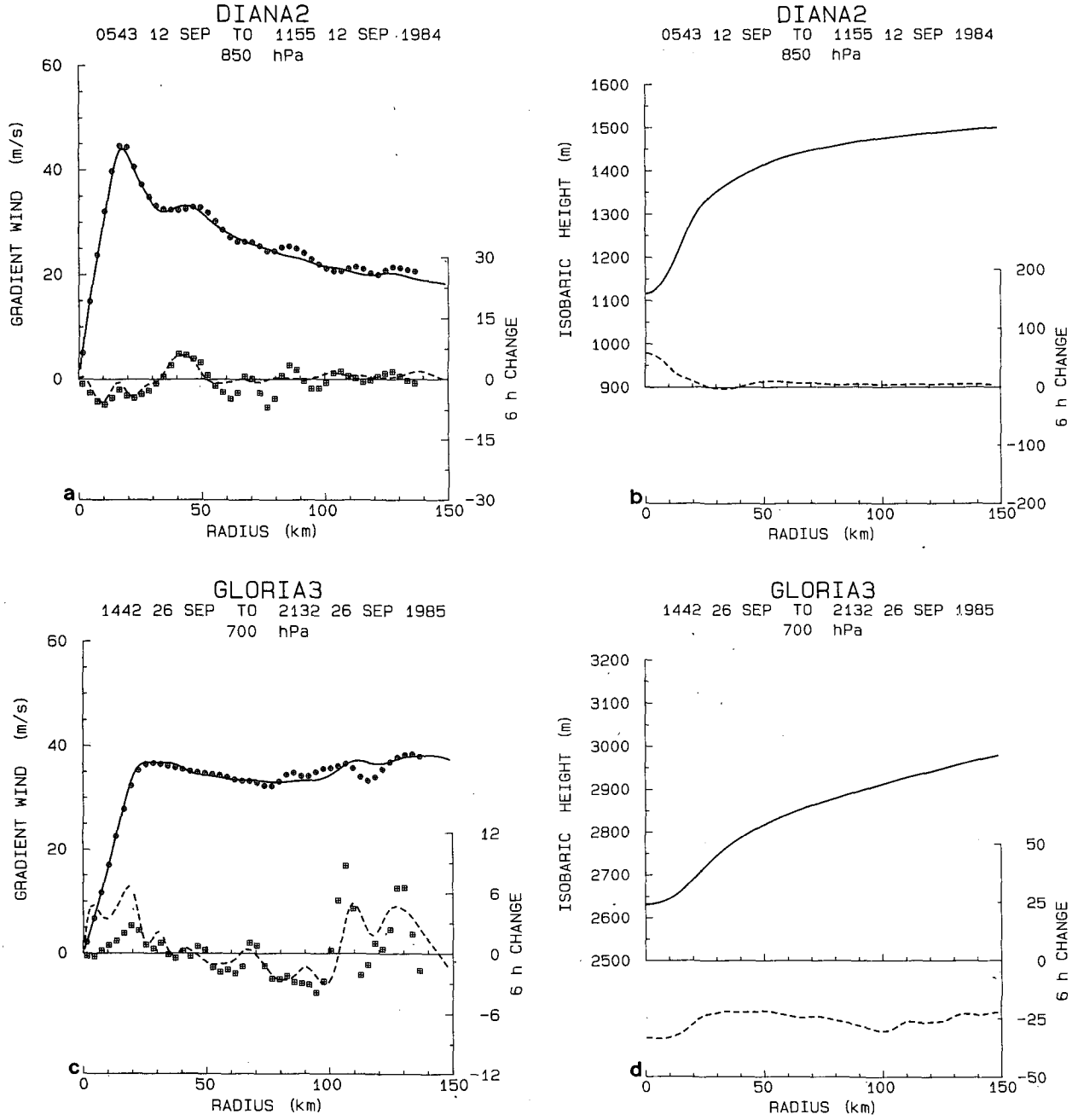

FIG. 5. Weakening hurricanes: (a) and (b) gradient balance and isobaric height observed during flight 840912H in Diana; and (c) and (d) during flight 850926H in Gloria. Data are represented in the same way as in Fig. 1.

increased the winds. Decreasing gradients of isobaric height and decreasing winds lay between the eyewall and the outer ring. In these weakening cases, the rms differences between $\bar{V}_g$ and $\bar{V}$ were 3% of the $\bar{V}_{\max}$ and between α_g and α_V were >30% of the maximum α_V.

Table 1 summarizes the differences between the observed and gradient winds in Figs. 1–5. Averaged over the 10 cases, the rms difference between $\bar{V}_g$ and $\bar{V}$ was <1.5 m s^{-1}; whereas the difference between α_g and α_V was 3.0 m s^{-1} per 6 h. The average wind difference for the sample represents individual cases reasonably well. Over the range of cyclone intensities, the RMS differences, although roughly constant in magnitude, were a decreasing fraction of the wind when the wind itself was stronger, representing >20% of $\bar{V}_{\max}$ in weak tropical storms but <2% of $\bar{V}_{\max}$ in intense hurricanes. The rms difference between $\bar{V}$ and $\bar{V}_g$ was smaller than that between $\bar{V}$ and the observed winds, about 5 m s^{-1} (Willoughby et al. 1984). The rms difference between α_g and α_V was typically 10%–30% of the maximum α_V. The lack of variation in the magnitudes with cyclone intensity suggests the rms differences may have stemmed largely from fixed uncertainty in determination of height gradients, rather than from actual agradient flow. The average $\bar{V} - \bar{V}_g$ had essentially zero bias, and $\alpha_g - \alpha_V$ had only a small bias, about 13% of the rms difference. Figures 1–5 show that the wind had no tendency to assume "supergradient" values at the RMW.

3. Discussion: Agradient winds

Observations in the preceding section establish gradient balance above the friction layer in the axisymmetric mean hurricane core. Scaling of the equations of motion for hurricane conditions shows that the axisymmetric swirling flow should be balanced, unless the acceleration of the radial flow is comparable with the centripetal acceleration (Shapiro and Willoughby 1982). The argument for balance applies only to the axisymmetric mean flow, because the observed motions at a particular position are the sum of the balanced vortex and asymmetric unbalanced motions, such as convection or waves.

On the other hand, axisymmetric unbalanced swirling motion could occur if the radial flow were strong or changed over a small spatial interval, making the radial acceleration large. The following is an idealized calculation of unbalanced primary flow caused by an imposed secondary flow in a steady, axisymmetric, cyclostrophic vortex. The calculation is based on the radial momentum equation:

$$\frac{d}{dr}\left(\frac{U^2}{2}\right) = \frac{d}{dr}\left(\frac{\gamma^2 V^2}{2}\right) = \frac{V^2}{r} - \frac{V_c^2}{r}. \tag{4}$$

V is the tangential (swirling) component of the flow; U is the radial component; $\gamma \equiv U/V$ is the tangent of the crossing angle; and V_c^2/r is the radial geopotential gradient, expressed in terms of the cyclostrophic wind. The strategy is to specify V_c, to "parameterize" the secondary circulation by specifying γ, and to solve (4) for U and V. The acyclostrophic flow is then $(V - V_c)$. The functional form chosen for γ is $(a - r)/r$. The trajectories, which crudely model the effects of friction or diabatic forcing, are logarithmic spirals converging toward $r = a$ from both the outside and inside.

$S = \exp\{-\int [2/(r\gamma^2)]dr\} = (r - a)^{-2} \exp[2a/(r - a]$ is an integrating factor for (4), such that:

$$\frac{d}{dr}\left(\frac{S\gamma^2 V^2}{2}\right) = \frac{d}{dr}\left(\frac{SU^2}{2}\right) = -\frac{SV_c^2}{r}. \tag{5}$$

Integration of (5) subject to the boundary condition $U(r_0) = U_0$ $(r_0 > a)$ yields:

$$\frac{SU^2}{2} - \frac{S_0 U_0^2}{2} = -\int_{r_0}^{r} \frac{SV_c^2}{r'}\, dr', \quad r \geq a \tag{6}$$

$$\frac{SU^2}{2} = -\int_{a}^{r} \frac{SV_c^2}{r'}\, dr \quad a \geq r. \tag{7}$$

Here r' is a dummy variable for integration and $S_0 = S(r_0)$. The different forms for U in $r \geq a$ and $r \leq a$ are necessary to make U continuous across $r = a$, where S is singular. As one approaches $r = a$ from $r > a$, $S \to \infty$; whereas as one approaches from $r < a$, $S \to 0$. Since application of l'Hospital's rule shows that ratio of the integral on the right to S behaves well at $r = a$ in both (6) and (7), U is bounded for any finite value of the constant of integration, $S_0 U_0$, in (6), but unbounded at $r = a$ for any nonzero value in (7). In order to evaluate the integrals numerically, it is necessary to remove the singularity of the integrand (e.g., Acton 1970) by adding and subtracting an analytically integrable function with the same singularity, in this case $S(r')V_c(a)/a$, so that in (6), for example:

$$\begin{aligned} &-\int_{r_0}^{r} S(r') \frac{V_c^2(r')}{r'}\, dr' \\ &= -\int_{r_0}^{r} S(r')\left[\frac{V_c^2(r')}{r'} - \frac{V_c^2(a)}{a}\right] dr' + \frac{V_c^2(a)}{2a^2} \\ &\quad \times \left[\exp\left(\frac{2a}{(r-a)}\right) - \exp\left(\frac{2a}{(r_0 - a)}\right)\right]. \end{aligned} \tag{8}$$

Once U is known, V can be calculated from

$$V^2 = V_c^2 + r\frac{d}{dr}\left(\frac{U^2}{2}\right),$$

or

$$V^2 = \frac{U^2}{\gamma^2}. \tag{9}$$

Figure 6 illustrates the solutions for a hurricane-like vortex. The wind components and radii are nondimensionalized by the maximum cyclostrophic wind and by the radius of maximum cyclostrophic wind.

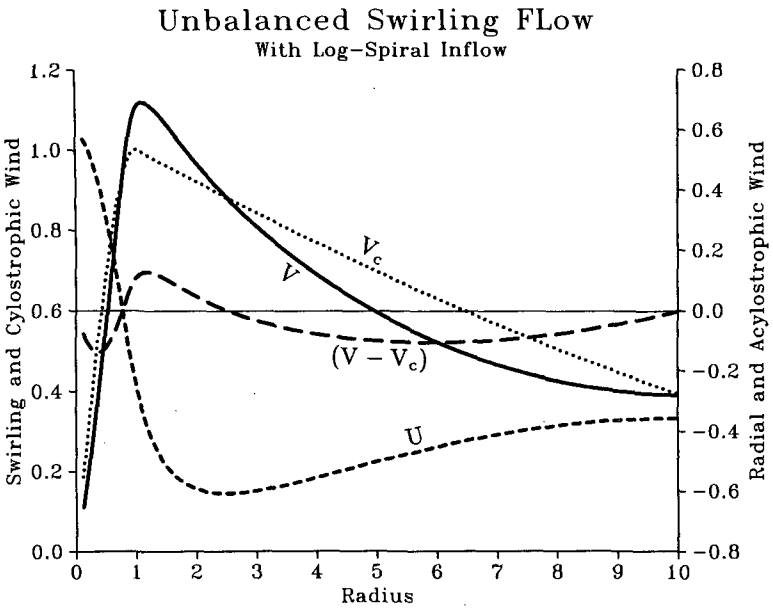

FIG. 6. Calculated nonbalanced wind in a specified cyclostrophic vortex with specified inflow angle such that the radial wind converges asymptotically to 0.8 times the radius of maximum cyclostrophic wind. The dotted curve represents the cyclostrophic wind, the solid curve the nonbalanced swirling wind, the shorter dashed curve the radial wind, and the longer dashed curve the difference between the balanced and nonbalanced wind. Wind components are nondimensionalized with the maximum balanced wind and radius is nondimensionalized with the radius of maximum balanced wind.

The asymptotic radius is just inside the RMW at $a = 0.8$. The inflow is stronger than one would expect in real hurricanes; for $r \gg a$, $\gamma = 1$, so that the inflow angle approaches 45° and $|U|$ approaches V. The maximum inflow is $U = 0.6$ at $r = 2.5$. Outside that radius, U accelerates toward the center—$d(U^2/2)/dr < 0$—and $V < V_c$; between $r = a$ and $r = 2.5$, U decelerates toward the center and $V > V_c$; for $r < a$, U decelerates away from the center and $V < V_c$. The maximum $|V - V_c|$ is 0.13. Thus $U^2/2$ acts like extra pressure: where $U^2/2$ increases away from the center, the winds are supercyclostrophic; where $U^2/2$ decreases away from the center, they are subcyclostrophic. In either case, the departures from balance are ~10% of the balanced wind.

A constant-depth axisymmetric frictional boundary layer (Shapiro 1983) provides a similar illustration of agradient flow. In the boundary layer, inward advection of angular momentum offsets frictional loss to the sea so that U is the ratio of the frictional torque to the radial gradient of angular momentum. Where the inflow passes under a wind maximum, the angular momentum gradient increases so that U decelerates. As in the previous analysis, retention of the deceleration in the radial momentum equation leads to theoretical prediction of supergradient flow on the inward side of the gradient-wind maximum, with some observational support (e.g., Mitsuta et al. 1988). In the theoretical analysis, the deceleration becomes discontinuous unless horizontal diffusion limits the tendency of advection to contract the spatial interval over which it takes place. In the constant-depth boundary layer with diffusion, U is roughly half as strong as in Fig. 6, but the more rapid deceleration makes the agradient flow comparable. These examples show a chain of cause and effect: diabatic or frictional forcing causes radial flow, and it is the accelerations of the radial flow—not of the swirling flow—that cause the unbalanced swirling.

4. Conclusions

Whatever the strengths or weaknesses of earlier studies arguing against balanced primary circulations in hurricanes, recent observations do not replicate their results. Analysis of a data obtained by INE-equipped aircraft during 977 penetrations or exits of the eyes in 19 hurricanes since 1977 shows that the gradient wind and gradient wind tendency are good approximations to the azimuthally averaged swirling wind and swirling wind tendency in the free atmosphere of the hurricane core. The root-mean-square difference between the observed tangential wind and the gradient wind is <1.5 m s^{-1}, and that between the tendencies is 3 m s^{-1} per 6 h.

The approximation is valid only in the azimuthal mean; no theoretical or observational reason exists to expect gradient balance locally. For example, the dynamics of the wavenumber 1 asymmetry appear to be

dominated by two inertial terms each an order of magnitude larger than the geopotential gradient (Willoughby 1988a). Thus, samples of a superposition of this asymmetry on an underlying balanced vortex would yield locally super- or subgradient wind. Moreover, theoretical analysis shows that nonbalanced flow will occur where the radial accelerations are large, for example, in the frictionally and diabatically induced convergence beneath the eyewall. Thus, although the balanced approximation is well established and supports a simple theoretical structure that explains a great deal, it is a conceptual starting point for study of more complicated situations rather than a comprehensive theory.

Acknowledgments. I want to express my thanks to everyone at the Hurricane Research Division and Aircraft Operations Center who participated in the research flights reported here. I also want to thank William Barry and M. Edward Rahn for help with computer programming and data analysis; Constance Arnhols for editorial assistance; and Chris Landsea, Katsuyuki Ooyama, Mark Powell, and Lloyd Shapiro for their comments on an earlier draft.

REFERENCES

Acton, F. S., 1970: *Numerical Methods That Work.* Harper & Row, 120–125.

Carrier, G. F., A. L. Hammond and O. D. George, 1971: A model of the mature hurricane. *J. Fluid Mech.*, **47,** 145–170.

Eliassen, A., 1952: Slow thermally or frictionally controlled meridional circulation in a circular vortex. *Astrophys. Norv.*, **5,** 19–60.

——, 1959: On the formation of fronts in the atmosphere. *The Atmosphere and Sea in Motion,* Bert Bolin, Ed., Rockefeller Institute Press, 277–287.

Emanuel, K. A., 1988: Toward a general theory of hurricanes. *Am. Scientist,* **76,** 371–379.

Gray, W. M., 1962: On the balance of forces and radial accelerations in hurricanes. *Quart. J. Roy. Meteor. Soc.*, **88,** 430–458.

——, 1967: The mutual variation of wind, shear, and baroclinicity in the cumulus convective atmosphere of the hurricane. *Mon. Wea. Rev.*, **95,** 55–73.

——, and D. J. Shea, 1973: The hurricane's inner core region. II. Thermal stability and dynamic characteristics. *J. Atmos. Sci.*, **30,** 1565–1576.

Hawkins, H. F., and D. T. Rubsam, 1968: Hurricane Hilda, 1964. II. Structure and budgets of the hurricane on October 1 1964. *Mon. Wea. Rev.*, **96,** 617–636.

Jorgensen, D. P., 1984: Mesoscale and convective-scale characteristics of mature hurricanes. Part II. Inner core structure of Hurricane Allen. *J. Atmos. Sci.*, **41,** 1287–1311.

Kuo, H. L., 1959: Dynamics of convective vortices and eye formation. *The Atmosphere and Sea in Motion,* Bert Bolin, Ed., Rockefeller Institute Press, 413–424.

LaSeur, N. E., and H. F. Hawkins, 1963: An analysis of Hurricane Cleo (1958) based on data from research reconnaissance aircraft. *Mon. Wea. Rev.*, **91,** 694–709.

Malkus, J. S., 1958: On the structure and maintenance of the mature hurricane eye. *J. Meteorol.*, **15,** 337–349.

Mitsuta, Y., T. Suenobu and T. Fujii, 1988: Supergradient surface winds in the eye of a typhoon. *J. Meteor. Soc. Japan.*, **66,** 505–508.

Palmen, E., 1956: Formation and development of tropical cyclones. *Proc. of the Tropical Cyclone Symposium,* Brisbane Bureau of Meteorology, Melbourne, 213–231.

Schubert, W. H., and J. J. Hack, 1982: Inertial stability and tropical cyclone development. *J. Atmos. Sci.*, **39,** 1687–1697.

Shapiro, L. J., 1983: The asymmetric boundary layer flow under a translating hurricane. *J. Atmos. Sci.*, **40,** 1984–1998.

——, and H. E. Willoughby, 1982: The response of balanced hurricanes to local sources of heat and momentum. *J. Atmos. Sci.*, **39,** 378–394.

Smith, R. K., 1981: The cyclostrophic adjustment of vortices with application to tropical cyclone modification. *J. Atmos. Sci.*, **38,** 2021–2030.

Willoughby, H. E., 1979: Forced secondary circulations in hurricanes. *J. Geophys. Res.*, **84,** 3173–3183.

——, 1988a: Linear motion of a shallow-water barotropic vortex. *J. Atmos. Sci.*, **45,** 1906–1928.

——, 1988b: The dynamics of the tropical cyclone core. *Aust. Meteor. Mag.*, **36,** 183–191.

——, 1990: Temporal changes of the primary circulation in tropical cyclones. *J. Atmos. Sci.*, **47,** 242–264.

——, J. A. Clos and M. G. Shoreibah, 1982: Concentric eyewalls, secondary wind maxima, and the evolution of the hurricane vortex. *J. Atmos. Sci.*, **39,** 395–411.

——, F. D. Marks and R. J. Feinberg, 1984: Stationary and moving convective bands in hurricanes. *J. Atmos. Sci.*, **41,** 3189–3211.